

Numerical implementation of the Loop-Tree Duality method

Sebastian Buchta,^a Grigorios Chachamis,^b Petros Draggiotis^c and Germán Rodrigo^a

^a*Instituto de Física Corpuscular, Universitat de València – Consejo Superior de Investigaciones Científicas, Parc Científic, E-46980 Paterna, Valencia, Spain.*

^b*Instituto de Física Teórica UAM/CSIC & Universidad Autónoma de Madrid, C/ Nicolás Cabrera 15, E-28049 Madrid, Spain*

^c*Institute of Nuclear and Particle Physics, NCSR "Demokritos", Agia Paraskevi, 15310, Greece*

E-mail: sbuchta@ific.uv.es, grigorios.chachamis@csic.es,
petros.draggiotis@gmail.com, german.rodriigo@csic.es

ABSTRACT: We present a first numerical implementation of the Loop-Tree Duality (LTD) method for the direct numerical computation of multi-leg one-loop Feynman integrals. We discuss in detail the singular structure of the dual integrands and define a suitable contour deformation in the loop three-momentum space to carry out the numerical integration. Then, we apply the LTD method to the computation of ultraviolet and infrared finite integrals, and present explicit results for scalar integrals with up to five external legs (pentagons) and tensor integrals with up to six legs (hexagons). The LTD method features an excellent performance independently of the number of external legs.

Contents

1	Introduction	1
2	Loop-tree duality at one-loop	3
3	The deformation of the contour	8
4	Results for multi-leg scalar one-loop integrals	10
4.1	Scalar triangles	11
4.2	Scalar Boxes	12
4.3	Scalar Pentagons	13
5	Tensor loop integrals	15
5.1	Tensor Pentagons	16
5.2	Tensor Hexagons	16
6	Conclusions	18
A	External momenta and internal masses of the sample points	19
A.1	Individual sample points	19
A.2	Energy and mass scans	23

1 Introduction

The recent discovery of the Higgs boson at the LHC represents a great success of the Standard Model (SM) of elementary particles. With the new run the primary goal is to study its properties in detail and to detect possible extensions to the SM. Precise theory predictions are needed to achieve this goal, which calls for calculations at the next-to-leading order (NLO) and beyond for multi-leg processes.

The development of automated NLO tools has seen great progress in recent years. Computing higher-order corrections in QFT, in particular in QCD and in the EW sector of the SM is highly challenging. The complexity increases as the number of external particles gets bigger and the order of the perturbative expansion. The task is far from trivial and each step presents its own difficulties: one needs first to generate the virtual and real scattering amplitudes, then carry out the integration over the loop momenta

for the virtual contribution and finally perform the phase-space integration for both real and virtual corrections after taking proper care so that the infrared divergencies cancel. In particular, infrared singularities of the virtual contribution can be subtracted by using appropriate semi-analytical terms and combine them with the ones stemming from the real corrections to produce finite results [1]. Purely numerical approaches on the integration of loop momenta have been discussed extensively in the literature [2–14]. The generation of amplitudes and calculation of cross-sections at one loop has seen great progress in recent years and algorithmic calculations at NLO are now considered standardised, based on purely numerical [15–17] and a mix of analytical and numerical approaches [18–20]. Substantial progress has also been made at higher orders [21–23].

The loop–tree duality (LTD) method [24–33] establishes that generic loop quantities (loop integrals and scattering amplitudes) in any relativistic, local and unitary field theory can be written as a sum of tree-level-like objects obtained after making all possible cuts to the internal lines of the corresponding Feynman diagrams, with one single cut per loop and integrated over a measure that closely resembles the phase-space of the corresponding real corrections [24, 25]. This duality relation is realised by a modification of the customary $+i0$ prescription of the Feynman propagators and encodes the causal structure of the scattering amplitudes in the expected way. The analysis of the singular behaviour of one-loop integrals and scattering amplitudes in this framework at the integrand level in the loop momentum space shows that there is a partial cancellation of singularities among different dual contributions such that physical infrared and threshold singularities remain restricted to a compact region of the loop three-momentum [28–30]. This feature opens up the intriguing possibility that virtual and real radiative corrections can be brought together under a common integral and be treated simultaneously with Monte Carlo techniques through a convenient mapping of the external momenta entering the virtual and real scattering amplitudes [33].

In this work, we present a first numerical implementation of the LTD method and we apply it to the computation of multi-leg one-loop scalar and tensor integrals. The outline of the paper is as follows. In Section 2 we review the LTD method at one-loop and discuss the singular behaviour of the dual integrand in the loop momentum space. In Section 3 we introduce the contour deformation in the loop three-momentum space which is used for the numerical loop integration. We present explicit numerical results for various external momenta configurations, in Section 4 for scalar integrals up to pentagons and in Section 5 for up to rank 3 tensor integrals with five and six external legs. Finally, our conclusions are presented in Section 6.

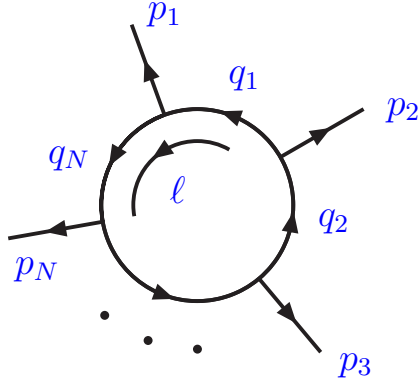


Figure 1: Momentum configuration of the one-loop N -point integral.

2 Loop-tree duality at one-loop

We consider a general one-loop N -leg scalar integral (see Fig. 1) in dimensional regularization, with d the number of space-time dimensions,

$$L^{(1)}(p_1, p_2, \dots, p_N) = \int_{\ell} \prod_{i \in \alpha_1} G_F(q_i), \quad \int_{\ell} \bullet = -i \int \frac{d^d \ell}{(2\pi)^d} \bullet, \quad (2.1)$$

where

$$G_F(q_i) = \frac{1}{q_i^2 - m_i^2 + i0} \quad (2.2)$$

are Feynman propagators that depend on the loop momentum ℓ , which flows anti-clockwise, and the four-momenta of the external legs p_i , $i \in \alpha_1 = \{1, 2, \dots, N\}$, which are taken as outgoing and are clockwise ordered. The momenta of the internal lines are denoted as $q_{i,\mu} = (q_{i,0}, \mathbf{q}_i)$, where $q_{i,0}$ is the energy (time component) and \mathbf{q}_i are the spatial components, which are defined as $q_i = \ell + k_i$ with $k_i = p_1 + \dots + p_i$, and $k_N = 0$ by momentum conservation. We also define $k_{ji} = q_j - q_i$ which, in fact, is independent of the loop momentum ℓ .

The corresponding dual representation of the scalar integral in Eq. (2.1) is obtained from the loop-tree duality (LTD) theorem [24]:

$$L^{(1)}(p_1, p_2, \dots, p_N) = - \sum_{i \in \alpha_1} \int_{\ell} \tilde{\delta}(q_i) \prod_{\substack{j \in \alpha_1 \\ j \neq i}} G_D(q_i; q_j), \quad (2.3)$$

where

$$G_D(q_i; q_j) = \frac{1}{q_j^2 - m_j^2 - i0 \eta k_{ji}}, \quad (2.4)$$

are dual propagators, η is an arbitrary future-like vector, i.e., a d -dimensional vector that can be either light-like ($\eta^2 = 0$) or time-like ($\eta^2 > 0$) with positive definite energy $\eta_0 \geq 0$, and

$$\tilde{\delta}(q_i) \equiv 2\pi i \theta(q_{i,0}) \delta(q_i^2 - m_i^2) , \quad (2.5)$$

selects the internal loop on-shell modes, $G_F^{-1}(q_i) = 0$, with positive definite energy, $q_{i,0} \geq 0$. Hence, the LTD theorem expresses the usual loop Feynman integral, Eq. (2.1), as a sum of single-cut phase-space integrals, Eq. (2.3), with

$$\int_{\ell} \tilde{\delta}(q_i) , \quad (2.6)$$

as the single-particle phase-space integration measure. The LTD theorem is valid not only for scalar one-loop integrals, but can straightforward be extended to deal with scattering amplitudes [24] and higher orders of the perturbative expansion [26, 27].

The integrand of the dual representation of one-loop integrals or scattering amplitudes feature certain types of singularities leading to ultraviolet, infrared or threshold singularities. This singular behaviour has already been thoroughly discussed in [29, 33]. We briefly recapitulate here the main points that are relevant in the present context.

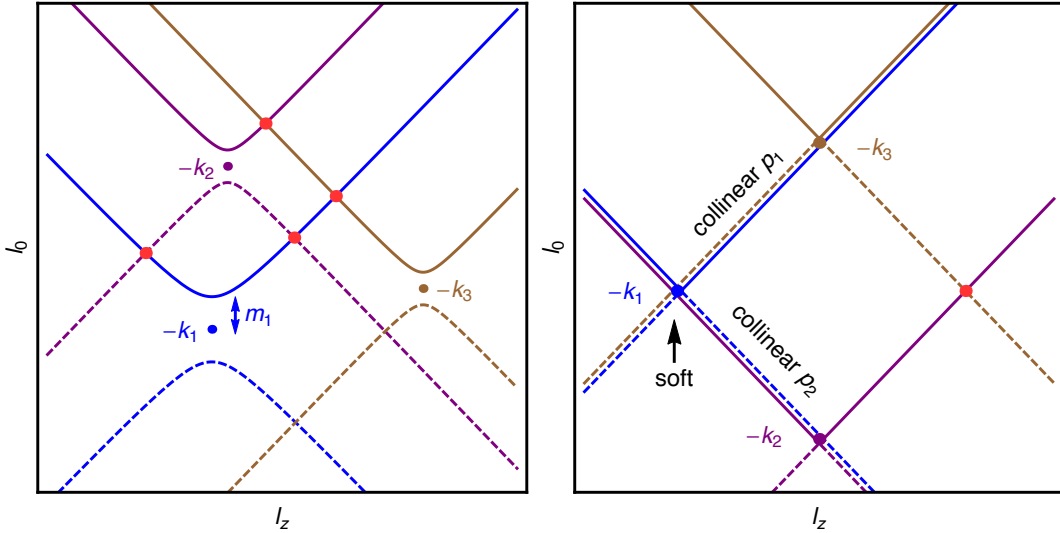


Figure 2: On-shell hyperboloids for three arbitrary propagators in Cartesian coordinates in the (l_0, l_z) space (left). Kinematical configuration with massless propagators leading to infrared singularities (right). In the latter case, the on-shell hyperboloids degenerate to light-cones.

For generic masses, the loop integrand in Eq. (2.1) becomes singular at the on-shell hyperboloids defined by $q_{i,0}^{(+)} = \sqrt{\mathbf{q}_i^2 + m_i^2} - i0$ (forward-hyperboloids, positive energy

mode) and $q_{i,0}^{(-)} = -\sqrt{\mathbf{q}_i^2 + m_i^2 - i0}$ (backward-hyperboloids, negative energy mode). This is illustrated in Fig. 2 for a given kinematical configuration with three internal loop propagators. Solid lines in Fig. 2 represent the forward on-shell hyperboloids, and dashed lines the backward on-shell hyperboloids. The LTD method is equivalent to evaluating the sum of the integrals along the forward on-shell hyperboloids with the singularities appearing at the intersection of each forward on-shell hyperboloid with the forward or backward on-shell hyperboloid of the other propagators. A crucial point of this discussion is the observation that dual propagators can be rewritten as

$$\tilde{\delta}(q_i) G_D(q_i; q_j) = i 2\pi \frac{\delta(q_{i,0} - q_{i,0}^{(+)})}{2q_{i,0}^{(+)}} \frac{1}{(q_{i,0}^{(+)} + k_{ji,0})^2 - (q_{j,0}^{(+)})^2}, \quad (2.7)$$

where $q_{i,0}^{(+)}$ can be interpreted as the loop energy measured along the forward on-shell hyperboloid with origin at $-k_i$. From Eq. (2.7) it is obvious that dual propagators become singular, $G_D^{-1}(q_i; q_j) = 0$, if one of the following conditions is fulfilled:

$$q_{i,0}^{(+)} + q_{j,0}^{(+)} + k_{ji,0} = 0, \quad (2.8)$$

$$q_{i,0}^{(+)} - q_{j,0}^{(+)} + k_{ji,0} = 0. \quad (2.9)$$

The first condition, Eq. (2.8), is satisfied if the forward on-shell hyperboloid of $G_F(q_i)$ intersects with the backward on-shell hyperboloid of $G_F(q_j)$. The second condition, Eq. (2.9), is true when the two forward on-shell hyperboloids intersect each other.

The solution to Eq. (2.8) is an ellipsoid in the loop three-momentum space and requires $k_{ji,0} < 0$. Moreover, since it is the result of the intersection of a forward with a backward on-shell hyperboloid the distance between the two propagators has to be future-like, $k_{ji}^2 \geq 0$. Actually, internal masses restrict this condition to

$$k_{ji}^2 - (m_j + m_i)^2 \geq 0, \quad k_{ji,0} < 0, \quad \text{forward with backward hyperboloids.} \quad (2.10)$$

The second equation, Eq. (2.9), leads to a hyperboloid in the loop three-momentum space, and there are solutions for $k_{ji,0}$ either positive or negative, namely when either of the two momenta is set on-shell. Here, the distance between the momenta of the propagators has to be space-like, although also time-like configurations can fulfill Eq. (2.9) as far as the time-like distance is small or close to light-like:

$$k_{ji}^2 - (m_j - m_i)^2 \leq 0, \quad \text{two forward hyperboloids.} \quad (2.11)$$

As it was demonstrated in [29], the integrand singularities appearing from the intersection of forward with forward on-shell hyperboloids cancel among dual contributions. To see that one needs to keep in mind that propagators are positive inside the on-shell

hyperboloids and negative outside. When integrating along the forward on-shell hyperboloids, every singularity is crossed twice. Firstly when going from the inside to the outside (or from the outside to the inside) and secondly from the outside to the inside (or from the inside to the outside). The crucial point is that the contributions coming from the two integrands have opposite sign and thus cancel out. Note that the imaginary dual prescription $\eta \cdot k_{ji}$ changes sign from the one dual contribution to the other to ensure the cancellation of the singularities. On the contrary, the singularities from the intersection of a forward with a backward on-shell hyperboloid survive because only a single dual contribution leads to that singularity and there is no possibility of cancellation. In the case of integrable singularities, a contour deformation can be employed as explained in the next section.

The action of the LTD can be encoded symbolically by the following matrix scheme

$$G_F \cdot G_F \cdots G_F \xrightarrow{\text{LTD}} \begin{pmatrix} \delta & G_D & G_D & \cdots & G_D \\ G_D & \delta & G_D & \cdots & G_D \\ G_D & G_D & \delta & \cdots & G_D \\ \vdots & \vdots & \vdots & \ddots & \vdots \\ G_D & G_D & G_D & \cdots & \delta \end{pmatrix} \quad (2.12)$$

Each line in the matrix to the right of the arrow in Eq. (2.12) represents a dual contribution with one single propagator on-shell, $\delta = \tilde{\delta}(q_i)$. The column index points to the corresponding dual propagators, $G_D = G_D(q_i; q_j)$. This scheme can now be used to graphically indicate the position of different singularities in a given dual integral. In Figs. 3 and 4 we apply it to a triangle and a box respectively. To be more specific, in Fig. 3 each of the 3D plots in the r.h.s represents the singularities of any one dual contribution. We plot the ellipsoid (orange surfaces) and hyperboloid (blue surfaces) singularities in the loop three-momentum space. The blue dots are the foci of the on-shell hyperboloids, i.e. $-\mathbf{k}_i$, $i \in \{1, 2, 3\}$. In the l.h.s, we see the singularity scheme, where the first line of the matrix corresponds to the first plot in the r.h.s, the second line corresponds to the second 3D plot and so on. In the matrix, an H indicates that the corresponding dual propagator from Eq. (2.12) generates an hyperboloid singularity, E stands for ellipsoid singularities, and zero means no singularity. Similarly, for a four-point function in Fig. 4.

In both cases, the hyperboloid singularities always appear pairwise across the dual contributions. This is not by accident. Due to the symmetry of Eq. (2.9) under the exchange of i (i counts dual contributions) and j (j counts leg positions) the hyperboloid singularities always appear in pairs and are distributed symmetrically around the main diagonal. Inspecting Eq. (2.8), which is the defining equation for ellipsoid singularities

we see that this equation is not symmetric under the exchange of indices. Thus for every ellipsoid singularity we have a zero as its counterpart.

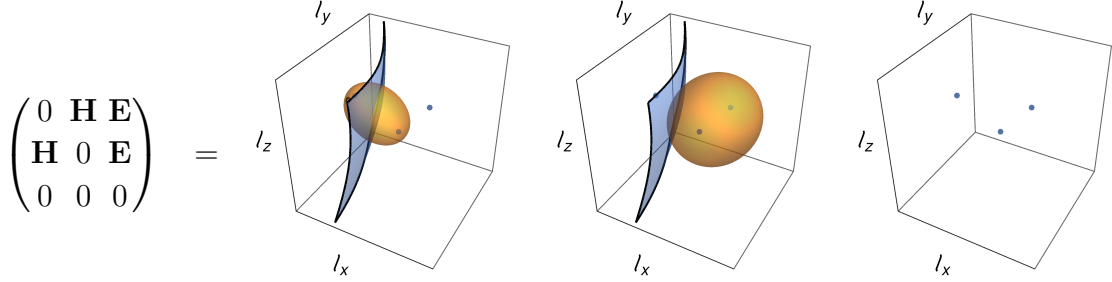


Figure 3: Singularity matrix of a sample three-point function and the corresponding singularity surfaces of the dual integrands in the loop three-momentum space.

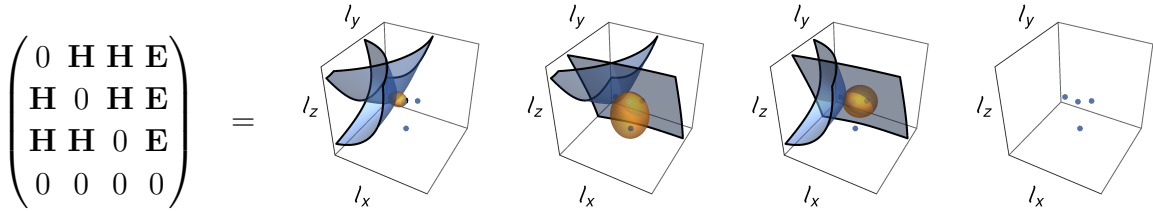


Figure 4: Singularity matrix of a sample four-point function and the corresponding singularity surfaces of the dual integrands in the loop three-momentum space.

At this point, we have established that the hyperboloid singularities do cancel among dual contributions and therefore we do not need to treat them in any special manner. Still though, they do have an impact on the way we need to deform our contour. This is due to the fact that in order to preserve the cancellation of hyperboloid singularities, dual contributions featuring the same hyperboloid singularity must receive the same deformation. To further illustrate this point, let us look at the pentagon example shown in Fig. 5. In Fig. 5, contributions one, two and three are coupled via their common hyperboloid singularities. Thus, they need to receive the very same deformation that accounts for all the ellipsoid singularities occurring within those contributions. These are found at position four of the second contribution and positions one and four of the third contribution. The fourth dual contribution is not coupled to any other contribution and a standalone deformation can be applied. The fifth contribution does not require any treatment.

$$\left. \begin{array}{l}
\left(\begin{array}{ccccc}
0 & \mathbf{H} & 0 & 0 & 0 \\
\mathbf{H} & 0 & \mathbf{H} & \mathbf{E} & 0 \\
\mathbf{E} & \mathbf{H} & 0 & \mathbf{E} & 0 \\
\mathbf{E} & \mathbf{E} & \mathbf{E} & 0 & \mathbf{E} \\
0 & 0 & 0 & 0 & 0
\end{array} \right) \\
\left. \begin{array}{l}
\left. \begin{array}{l}
\rightarrow \\
\rightarrow
\end{array} \right\} \\
\rightarrow \\
\rightarrow
\end{array} \right\}
\begin{array}{l}
\text{Contributions are coupled:} \\
\text{Every contribution receives all deformations} \\
\text{that occur within the group.} \\
\text{Deform with ellipsoids that itself contains.} \\
\text{No deformation needed here.}
\end{array}
\end{array}
\right.$$

Figure 5: Five-point function with dual contributions coupled by hyperboloid singularities.

As a general strategy, one organises the dual contributions into groups. A group is a set of pairwise coupled contributions. To each of the groups a contour deformation is applied independently from the others. Within a group every contribution receives the same deformation that accounts for all the ellipsoids of the group. Turning back to the example in Fig. 5, we have three groups: the first group involves contributions one to three, the second group is contribution four and the third group is contribution five.

3 The deformation of the contour

As we saw in Section 2, the ellipsoid singularities (forward–backward type) lead to integrable threshold singularities that lie on the real axis. To deal with them, we need to deform the integration path into the imaginary space. Every valid deformation must satisfy a certain set of requirements [3]:

1. The deformation has to respect the $i0$ -prescription of the propagator. In general, a contour deformation in the loop three-momentum space has the form:

$$\ell \rightarrow \ell' = \ell + i\boldsymbol{\kappa} . \quad (3.1)$$

where $\boldsymbol{\kappa}$ is a function of the loop momentum ℓ and the external momenta. In our case, we want to perform the integration over a product of dual propagators. Inserting Eq. (3.1) into the on-shell energy relation, we obtain

$$q_{i,0}^{(+)} = \sqrt{-\boldsymbol{\kappa}^2 + 2i\boldsymbol{\kappa} \cdot \mathbf{q}_i + \mathbf{q}_i^2 + m_i^2 - i0} . \quad (3.2)$$

The $i0$ -prescription tells us in which direction to deform when coming close to a singularity. Hence, any valid deformation must match this prescription. Consequently we need to have

$$\boldsymbol{\kappa} \cdot \mathbf{q}_i < 0 . \quad (3.3)$$

2. The deformation should vanish at infinity: We are looking for a deformation that does not change the actual value of the integral. We do not want $|\kappa|$ to grow for $|\ell| \rightarrow \infty$. An easy way to satisfy this condition is to choose κ such that $|\kappa| \rightarrow 0$ as $|\ell| \rightarrow \infty$.¹

With these conditions in mind, we construct the deformation in the following way: As explained in Section 2, we first organise the dual contributions into groups. For every ellipsoid singularity of the group we include a factor:

$$\lambda_{ij} \left(\frac{\mathbf{q}_i}{\sqrt{\mathbf{q}_i^2}} + \frac{\mathbf{q}_j}{\sqrt{\mathbf{q}_j^2}} \right) \exp \left(-\frac{G_D^{-2}(q_i; q_j)}{A_{ij}} \right), \quad (3.4)$$

with $\mathbf{q}_i = \ell + \mathbf{k}_i$ and ℓ the loop three-momentum. The deformation factor in Eq. (3.4) consists of two main components. The first component defines the direction of the deformation, and is given by the sum of the two unit vectors $\mathbf{q}_i/\sqrt{\mathbf{q}_i^2}$ and $\mathbf{q}_j/\sqrt{\mathbf{q}_j^2}$. As shown in Fig. 6 the vectors \mathbf{q}_i and \mathbf{q}_j have their origin in $-\mathbf{k}_i$ and $-\mathbf{k}_j$, respectively, and the deformation is designed to point to the outside of the singularity ellipsoid. For an efficient numerical implementation, however, we should also take into account in the selection of the deformation parameters that for massive propagators the vectors $-\mathbf{k}_i$ and $-\mathbf{k}_j$ might be slightly displaced from the true focal points of the ellipsoid. Inside the ellipsoid, the sum of the two unit vectors $\mathbf{q}_i/\sqrt{\mathbf{q}_i^2}$ and $\mathbf{q}_j/\sqrt{\mathbf{q}_j^2}$ helps to flatten the deformation and indeed they cancel each other along the major axis of the ellipsoid. By choosing all the scaling parameters $\lambda_{ij} < 0$ for all possible combinations $\{ij\}$ we satisfy the first condition in Eq. (3.3).

The second component in Eq. (3.4) is the exponential factor $\exp(-G_D^{-2}(q_i; q_j)/A_{ij})$ that suppresses the deformation at infinity. At singular points, $G_D^{-2}(q_j; q_i)$ vanishes and thus the deformation reaches its maximum. Far away from the singularity, $-G_D^{-2}(q_j; q_i)$ reaches a large negative value and thus the exponential tends rapidly to zero. Finally, the factor λ_{ij} is a scaling factor, and A_{ij} determines the width of the deformation. The indices ij in λ_{ij} and A_{ij} indicate that those parameters can be selected individually for each deformation contribution for optimization purposes. Then, we sum over the

¹ Strictly speaking, there is a third condition. The deformation must vanish at the position of soft or collinear singularities. This point is of importance for the matching of soft and collinear singularities between real and virtual corrections [33]. If the deformation shifts those singularities together with everything else, the cancellation will be spoiled. However, in the scope of this article, we are only dealing with infrared finite diagrams.

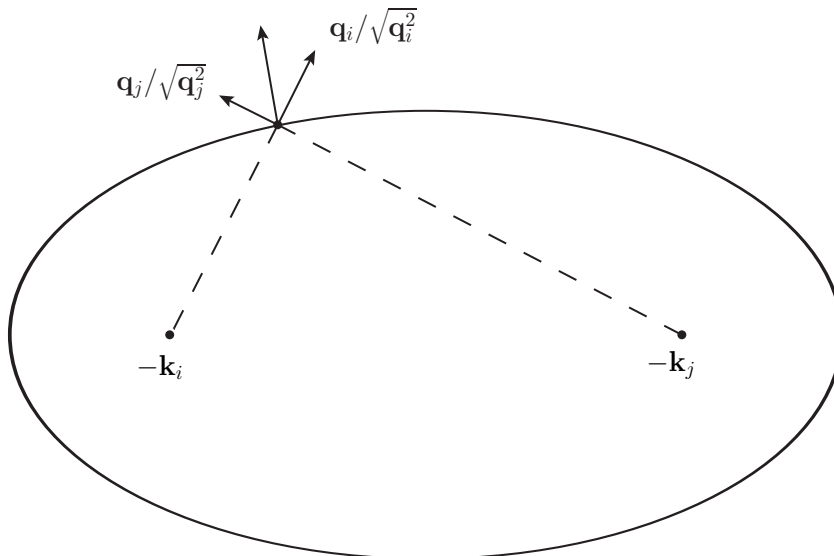


Figure 6: Two-dimensional slice of the ellipsoid singularity of dual contribution i at position j . The resulting vector gives the direction of the deformation.

entire group of coupled singularities and arrive at:

$$\kappa = \sum_{i,j \in \text{group}} \lambda_{ij} \left(\frac{\mathbf{q}_i}{\sqrt{\mathbf{q}_i^2}} + \frac{\mathbf{q}_j}{\sqrt{\mathbf{q}_j^2}} \right) \exp \left(-\frac{G_D^{-2}(q_j; q_i)}{A_{ij}} \right). \quad (3.5)$$

The corresponding Jacobian can be calculated analytically or numerically; in our current implementation we have chosen the analytic way.

4 Results for multi-leg scalar one-loop integrals

We have implemented the LTD method in a C++ code and all the results in this paper were obtained on a desktop machine with an Intel i7 (3.4GHz) processor with 8 cores and 16 GB of RAM. The program uses the Cuba library [35] as a numerical integrator. The user needs only to input the number of external legs, the external momenta, the internal masses and has the freedom to change the parameters of the contour deformation. The momenta and masses can be read in from a text file. The user can choose between Cuhre [36, 37] and VEGAS [38], and give the desired number of evaluations. At run time, the code performs the following steps:

1. Reads in masses and external momenta.

2. Checks where ellipsoid singularities occur.
3. Checks where hyperboloid singularities occur, groups the dual contributions accordingly and applies the contour deformation.
4. Calls the integrator.

We use `MATHEMATICA 10.0` [39] to generate random momenta and masses to scan as much of the phase-space as possible, to ensure that the program works properly in all regions. For our numerical results, the routine `Cuhre` was used unless otherwise stated. The momenta and masses of all the sample phase-space points used in the following sections are collected in Appendix A. We mainly used `LoopTools 2.10` [34] and also `SecDec 3.0` [40] to produce reference results to compare with.

4.1 Scalar triangles

We consider first infrared finite scalar triangle integrals. The sample point P1 in Table 1 has all internal masses equal while P2 has three different internal masses. Momenta and masses were chosen randomly between -100 GeV and $+100$ GeV. Similarly, P3 in Table 1 has all internal masses equal whereas in P4 all three of them have different values.

Points with momentum configurations that do not need deformation (i.e. whose loop integral is purely real) are computed in well below one second with a precision of at least 4 digits. For points with momentum configurations that require deformation, the calculation time increases to typically 3 – 15 seconds.

	Scalar Triangle	Real Part	Imaginary Part
P1	LoopTools	-5.85694×10^{-5}	
	LTD	$-5.85685(24) \times 10^{-5}$	
P2	LoopTools	-3.39656×10^{-7}	
	LTD	$-3.39688(53) \times 10^{-7}$	
P3	LoopTools	5.37305×10^{-4}	$-i 6.68103 \times 10^{-4}$
	LTD	$5.37307(9) \times 10^{-4}$	$-i 6.68103(9) \times 10^{-4}$
P4	LoopTools	-5.61370×10^{-7}	$-i 1.01665 \times 10^{-6}$
	LTD	$-5.61363(83) \times 10^{-7}$	$-i 1.01666(8) \times 10^{-6}$

Table 1: Sample scalar triangles.

An important check of our implementation is the mass-scan around threshold. In Fig. 7 all internal masses are equal, i.e. $m_i = m$, $i \in \{1, 2, 3\}$, and the center-of-mass

energy s was kept constant while varying the mass m . The calculation time remains constant for all mass values.

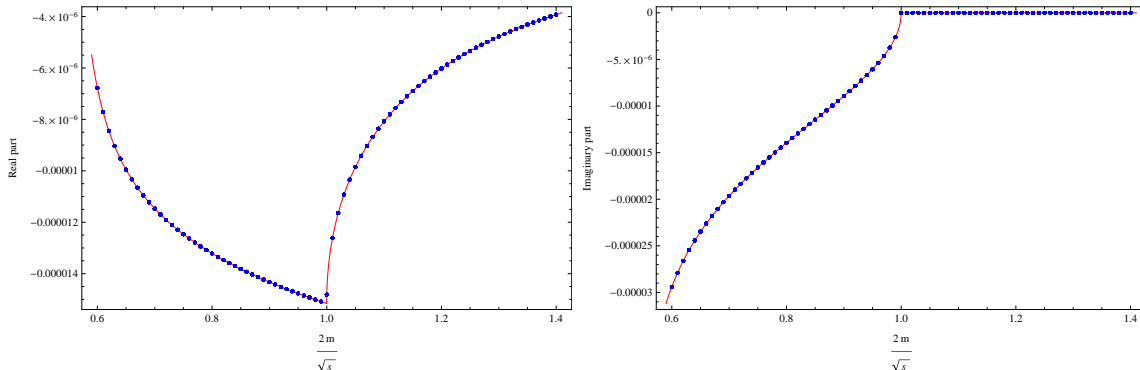


Figure 7: Mass scan of the region around threshold. The red curve is done with LoopTools and the blue points are obtained with the LTD method.

4.2 Scalar Boxes

Next we consider infrared finite box scalar integrals. To get good precision (4 digits), for boxes that need deformation we use 4 to $5 \cdot 10^6$ Cuhre calls, whereas for phase-space points with no deformation only $5 \cdot 10^4$ calls, the same as in the triangle case. This is reflected in the running times. Points with deformation require about 15 seconds whereas points with no deformation well below one second. While it is practically guaranteed to get the no-deformation points with good precision, for points with deformation the quality of results depends on the proper choice of the deformation parameters. Therefore, we mainly focus our attention to such points in the following. The sample points P5 and P7 of Table 2 correspond to a momentum configuration in which all four internal masses are equal. In P6 and P8 all masses are different. In P9 two adjacent internal lines have equal masses as well as the two opposing ones. P10 represents a situation in which opposite lines have equal masses.

We perform again a mass-scan (see Fig. 8) with all internal masses equal, i.e. $m_i = m, i \in 1, 2, 3, 4$. The center-of-mass energy s was kept constant while the mass m was varied. The program deals well with all kinds of boxes, even when many different kinematical scales are involved. In Fig. 8, two thresholds are crossed at $2m/\sqrt{s} = 0.65$ and 1. From right to left, the number of ellipsoid singularities grows by one after each threshold is crossed, starting from one to end up to three.

		Real Part	Imaginary Part
P5	LoopTools	2.15339×10^{-13}	
	LTD	$2.15319(52) \times 10^{-13}$	
P6	LoopTools	1.39199×10^{-11}	
	LTD	$1.39199(6) \times 10^{-11}$	
P7	LoopTools	-2.38766×10^{-10}	-3.03080×10^{-10}
	LTD	$-2.38775(76) \times 10^{-10}$	$-3.03063(76) \times 10^{-10}$
P8	LoopTools	-4.27118×10^{-11}	4.49304×10^{-11}
	LTD	$-4.27120(95) \times 10^{-11}$	$4.49307(95) \times 10^{-11}$
P9	LoopTools	-7.37897×10^{-11}	-1.19657×10^{-10}
	LTD	$-7.37916(782) \times 10^{-11}$	$-1.19649(78) \times 10^{-10}$
P10	LoopTools	-1.85544×10^{-10}	2.13553×10^{-10}
	LTD	$-1.85548(8) \times 10^{-10}$	$2.13554(8) \times 10^{-10}$

Table 2: Sample scalar boxes.

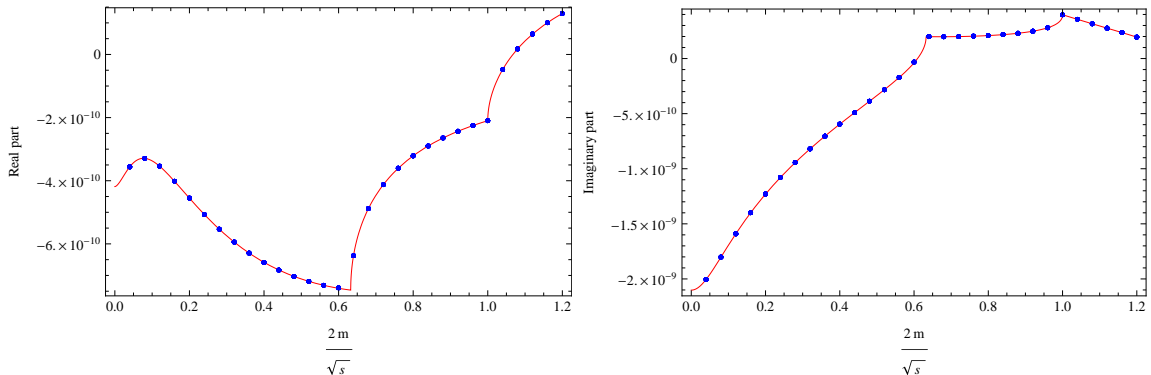


Figure 8: Mass-scan of a box integral. The red curve is done with LoopTools and the blue points are obtained with the LTD method.

4.3 Scalar Pentagons

Let us now turn to pentagon diagrams. No-deformation points are computed with 10^5 evaluations which takes about 0.5 seconds. Points with deformation demand $5 \cdot 10^6$ evaluations to maintain the level of precision of the triangles and boxes. This results to an average calculation time of about 30 seconds.

In Table 3 we display a collection of pentagon example results for different kinematical configurations. In P11 and P13 all internal masses are equal; in P14 they

	Scalar Pentagon	Real Part	Imaginary Part
P11	LoopTools	-1.24025×10^{-13}	
	LTD	$-1.24027(16) \times 10^{-13}$	
P12	LoopTools	-1.48356×10^{-14}	
	LTD	$-1.48345(116) \times 10^{-14}$	
P13	LoopTools	1.02350×10^{-11}	$+i 1.40382 \times 10^{-11}$
	LTD	$1.02353(1) \times 10^{-11}$	$+i 1.40385(1) \times 10^{-11}$
P14	LoopTools	-1.52129×10^{-15}	$-i 1.17401 \times 10^{-14}$
	LTD	$-1.52657(602) \times 10^{-15}$	$-i 1.17483(60) \times 10^{-15}$
P15	LoopTools	-4.29464×10^{-15}	$-i 6.55440 \times 10^{-14}$
	LTD	$-4.29520(845) \times 10^{-15}$	$-i 6.55433(85) \times 10^{-14}$

Table 3: Sample scalar pentagons.

are all distinct from each other and in P15 we have $m_1 = m_2 = m_3 \neq m_4 = m_5$. Our implementation of the LTD method shows its robustness by producing accurate results regardless of the kinematical situation. This statement is further supported by an energy-scan which we performed and which is shown in Fig. 9. The center-of-mass energy s is varied. This is realized by varying p_3 while keeping p_3^2 constant. Of course, due to momentum conservation, this involves $p_4^2 = (p_1 + p_2 + p_3)^2$ not being constant. In this scan, we cross three thresholds at $s \approx -8.5 \cdot 10^3$, $-13.5 \cdot 10^3$ and $-21 \cdot 10^3$ GeV² which divide the scan into four zones. From right to left, we start with zero ellipsoid singularities in the first zone, then we have one in the second zone, two in the third zone and finally one in the leftmost zone.

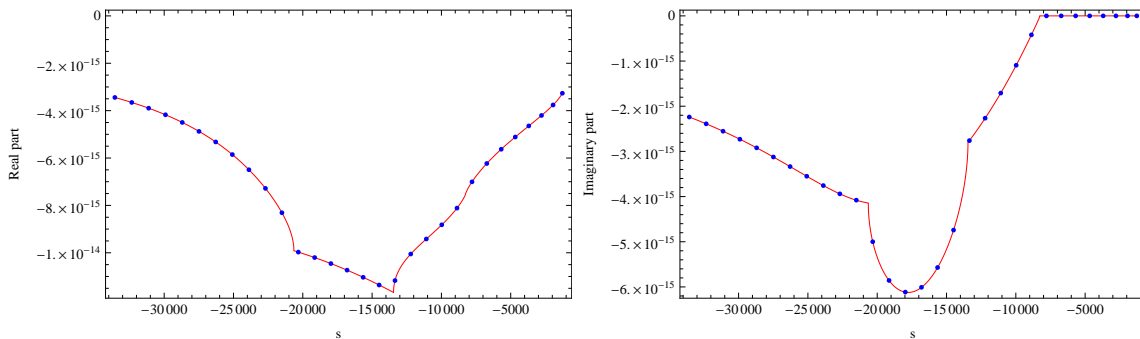


Figure 9: Energy-scan of a scalar pentagon. The red curve is done with LoopTools and the blue points are obtained with the LTD method.

5 Tensor loop integrals

The LTD relation for scalar loop integrals can easily be extended to deal tensor integrals. As long as the quantum field theory is local and unitary, these tensor factors do not lead to additional singularities [24] and the LTD method can then be applied in a straightforward manner. If the one-loop integral features a non-trivial numerator $\mathcal{N}(\ell, \{p_i\})$,

$$L^{(1)}(p_1, \dots, p_N; \mathcal{N}(\ell, \{p_i\})) = \int_{\ell} \mathcal{N}(\ell, \{p_i\}) \prod_{i \in \alpha_1} G_F(q_i) , \quad (5.1)$$

then, the LTD theorem takes the form

$$L^{(1)}(p_1, \dots, p_N; \mathcal{N}(\ell, \{p_i\})) = - \sum_{i \in \alpha_1} \int_{\ell} \tilde{\delta}(q_i) \mathcal{N}(\ell, \{p_i\}) \prod_{\substack{j \in \alpha_1 \\ j \neq i}} G_D(q_i; q_j) . \quad (5.2)$$

While the numerator is formally left unchanged, there is actually a potential implication. The presence of the dual delta function demands $q_{i,0}^{(+)} = \sqrt{\mathbf{q}_i^2 + m_i^2 - i0}$, which is equivalent to

$$\ell_0 = -k_{i,0} + \sqrt{\mathbf{q}_i^2 + m_i^2 - i0} . \quad (5.3)$$

In other words, whenever we perform a single cut of a Feynman graph, the numerator has to be evaluated at the position of the cut which is fixed by the dual delta function. As a direct consequence, the numerator takes a different form in each dual contribution.

Another important aspect to take into consideration is the cancellation of singularities among dual contributions. Here, we would like to make explicit that the numerators do not spoil the cancellation of the hyperboloid singularities. A typical numerator is a polynomial of scalar products of the loop-momentum with external momenta: $\ell \cdot p_k$. Let us see what happens to a single factor when it hits the singularity. Note first, that the hyperboloid singularity is given by Eq. (2.9) which we rewrite in the more suitable form

$$q_{i,0}^{(+)} - k_{i,0} = q_{j,0}^{(+)} - k_{j,0} . \quad (5.4)$$

Using Eq. (5.3), the loop-momentum ℓ contracted with some external momentum p_k is:

$$\ell \cdot p_k \big|_{i\text{-th cut}} = (q_{i,0}^{(+)} - k_i) p_{k,0} - \boldsymbol{\ell} \cdot \mathbf{p}_k = (q_{j,0}^{(+)} - k_j) p_{k,0} - \boldsymbol{\ell} \cdot \mathbf{p}_k = \ell \cdot p_k \big|_{j\text{-th cut}} , \quad (5.5)$$

where we have used Eq. (5.4). This means that the numerators of two dual contributions i and j take the same value at their common pole, thus leaving the cancellation of

hyperboloid singularities intact. This is an important property to take advantage of, because it allows us to straightforwardly apply the LTD method to such diagrams without any additional effort.

5.1 Tensor Pentagons

Next, we investigate tensor pentagon integrals at the one-loop level with numerators up to rank three. The number of evaluations is chosen to be the same as in the scalar case, i.e. 10^5 times for no-deformation points and $5 \cdot 10^6$ times for phase-space points that require deformation. This results in calculation times of about 1 second and 30 seconds, respectively.

In Table 4 we show a selection of sample points. The reference points P16 and P18 feature the rank two numerator $(\ell \cdot p_3) \times (\ell \cdot p_4)$ while P17 and P19 have the numerator $(\ell \cdot p_3) \times (\ell \cdot p_4) \times (\ell \cdot p_5)$. All the points have all internal masses equal. P19 actually contains six ellipsoid singularities whereas the other sample points have two to three. We include this point to demonstrate that the program does well even under such challenging circumstances.

For tensor pentagons and hexagons, we have used the program SecDec [40] to cross-check our results. We have run SecDec taking no care to optimise its runtime. This means that in the following, whenever we present the running times of SecDec we do it for completeness reasons and not because we imply that our code compares better or worse to SecDec. A proper comparison of our implementation with available codes is beyond the scope of this paper.

We have performed several different scans; a sample is presented in Fig. 10. In this energy-scan, we varied p_1 and thus the center-of-mass energy $s = (p_1 + p_2)^2$, similar to what we have done with scalar pentagons. The corresponding numerator function is $(\ell \cdot p_1) \times (\ell \cdot p_2) \times (\ell \cdot p_3)$, which means that both numerator and denominator change in the scan. In Fig. 10, one can see that the LTD method is able to successfully pass this test.

5.2 Tensor Hexagons

Finally, we compute hexagon tensor integrals. The number of evaluations for no-deformation points is 10^6 and for deformation points $8 \cdot 10^6$. The typical corresponding computation times are about 10 and 75 seconds, respectively. Since LoopTools can provide results only up to pentagons, we used exclusively here the program SecDec to cross-check.

We present a selection of sample points in Table 5. P20 and P22 feature the rank one numerator $\ell \cdot p_1$, the former has all internal masses different, in the latter they are all equal. P21 has six distinct internal masses and the numerator function

	Rank	Tensor Pentagon	Real Part	Imaginary Part	Time [s]
P16	2	LoopTools	-1.86472×10^{-8}		
		SecDec	$-1.86471(2) \times 10^{-8}$		45
		LTD	$-1.86462(26) \times 10^{-8}$		1
P17	3	LoopTools	1.74828×10^{-3}		
		SecDec	$1.74828(17) \times 10^{-3}$		550
		LTD	$1.74808(283) \times 10^{-3}$		1
P18	2	LoopTools	-1.68298×10^{-6}	$+i 1.98303 \times 10^{-6}$	
		SecDec	$-1.68307(56) \times 10^{-6}$	$+i 1.98279(90) \times 10^{-6}$	66
		LTD	$-1.68298(74) \times 10^{-6}$	$+i 1.98299(74) \times 10^{-6}$	36
P19	3	LoopTools	-8.34718×10^{-2}	$+i 1.10217 \times 10^{-2}$	
		SecDec	$-8.33284(829) \times 10^{-2}$	$+i 1.10232(107) \times 10^{-2}$	1501
		LTD	$-8.34829(757) \times 10^{-2}$	$+i 1.10119(757) \times 10^{-2}$	38

Table 4: Tensor pentagons involving numerators of rank two and three.

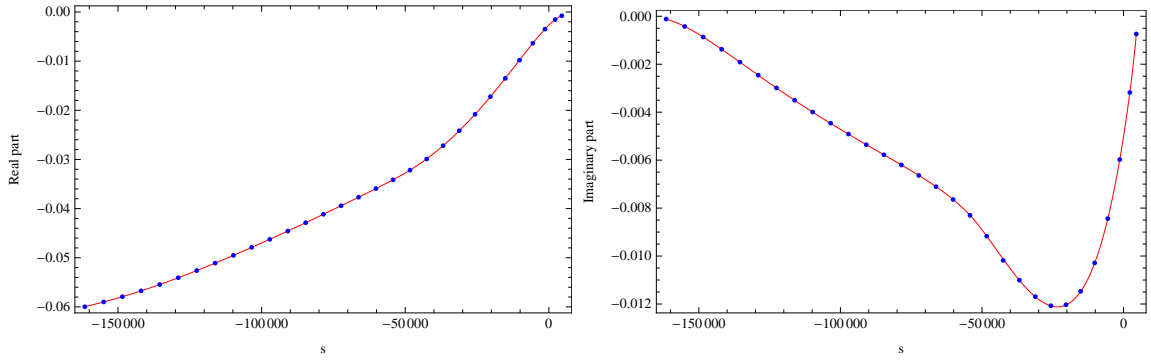


Figure 10: Energy-scan of a rank three tensor pentagon around the threshold region. The red curve is done with LoopTools and the blue points are obtained with the LTD method.

$(\ell \cdot p_2) \times (\ell \cdot p_4) \times (\ell \cdot p_6)$, **P23** possesses the numerator $(\ell \cdot p_2) \times (\ell \cdot p_5)$ and six different masses, as well. Finally, **P24** has all momenta distinct from each other and exhibits the numerator $(\ell \cdot p_4) \times (\ell \cdot p_5) \times (\ell \cdot p_6)$.

	Rank	Tensor Hexagon	Real Part	Imaginary Part	Time[s]
P20	1	SecDec	$-1.21585(12) \times 10^{-15}$		36
		LTD	$-1.21552(354) \times 10^{-15}$		6
P21	3	SecDec	$4.46117(37) \times 10^{-9}$		5498
		LTD	$4.461369(3) \times 10^{-9}$		11
P22	1	SecDec	$1.01359(23) \times 10^{-15}$	$+i 2.68657(26) \times 10^{-15}$	33
		LTD	$1.01345(130) \times 10^{-15}$	$+i 2.68633(130) \times 10^{-15}$	72
P23	2	SecDec	$2.45315(24) \times 10^{-12}$	$-i 2.06087(20) \times 10^{-12}$	337
		LTD	$2.45273(727) \times 10^{-12}$	$-i 2.06202(727) \times 10^{-12}$	75
P24	3	SecDec	$-2.07531(19) \times 10^{-6}$	$+i 6.97158(56) \times 10^{-7}$	14280
		LTD	$-2.07526(8) \times 10^{-6}$	$+i 6.97192(8) \times 10^{-7}$	85

Table 5: Tensor hexagons involving numerators of rank one to three.

6 Conclusions

The Loop-Tree Duality has many appealing theoretical properties for the calculation of processes with many external legs. In this paper, we have investigated the practicability of a first numerical implementation of the LTD method.

In our analysis of the singular behaviour of the loop integrand, we found two distinct types of singularities: Ellipsoid singularities which require the application of contour deformation and hyperboloid singularities that occur pairwise and cancel among different dual contributions. In order to preserve their cancellation, dual contributions featuring the same hyperboloid singularity pair must receive the same contour deformation. This leads to the following algorithm: Sets of pairwise coupled dual contributions are organized into groups. Each group is deformed independently from the others and each dual contribution of such a group receives the exact same contour deformation that accounts for all the ellipsoid singularities of the entire group.

We applied a contour deformation that efficiently deals with the ellipsoid singularities by meeting all the important criteria [3]. This setup has been successful in the calculation of finite multi-leg scalar and tensor integrals. We found the results to be in very good agreement with the reference values produced by LoopTools and SecDec. An important further check of our implementation presented here was various scans which show that the code handles equally well broad slices of the phase space. The code excels in cases that involve many external legs as it shows a modest increase in running times in comparison to cases with fewer legs. From this first study, we can be optimistic that our implementation of the LTD method offers a competitive alternative

for computing multi-scale, multi-leg scalar and tensor one-loop integrals.

In this paper we have only considered IR- and UV-finite integrals. However, the treatment of IR- and UV-divergent graphs in the context of the LTD method and the description of how to combine directly the virtual with the real radiative corrections in order to obtain an infrared finite implementation has been presented recently [33]. The extension of our code to deal with these cases is an ongoing project.

Acknowledgements

We thank S. Catani for a longstanding fruitful collaboration. We also thank S. Borowka and G. Heinrich for their help in running SecDec. This work has been supported by the Research Executive Agency (REA) under the Grant Agreement No. PITN-GA-2010-264564 (LHCPhenoNet), by the Spanish Government and ERDF funds from the European Commission (Grants No. FPA2014-53631-C2-1-P, FPA2011-23778, FPA2013-44773-P), and by Generalitat Valenciana under Grant No. PROMETEOII/2013/007. G.C. acknowledges support from Marie Curie Actions (PIEF- GA-2011-298582). S.B. acknowledges support from JAEPre programme (CSIC). P.D. acknowledges support from General Secretariat for Research and Technology of Greece and from European Regional Development Fund MIS-448332-ORASY (NSRF 2007-13 ACTION, KRIPIS).

A External momenta and internal masses of the sample points

Here we give the external momenta and internal masses of the different phase-space points and scans shown in Sections 4 and 5. Due to momentum conservation $p_N = -\sum_{i=1}^{N-1} p_i$, it is sufficient to give only the momenta p_1 to p_{N-1} . Momenta and masses are implicitly given in GeV.

To produce the energy scans (Fig. 9 and Fig. 10), we varied the external momentum p_1 by multiplying with the square root of some scaling parameter λ (not to be confused with the scaling parameter λ_{ij} of the contour deformation). This is indicated where we give the respective momenta.

A.1 Individual sample points

Figure 3 $p_1 = (44.38942, 17.84418, 12.70440, -23.67441)$
 $p_2 = (11.62982, -35.11756, -9.52573, 1.27635)$
 $m_1 = m_2 = m_3 = 7.89824$

Figure 4 $p_1 = (95.95213, 65.25140, -40.62468, 30.93648)$
 $p_2 = (68.47023, -60.09584, 18.23998, 84.29507)$

- $p_3 = (12.99839, 12.08603, -99.08246, -34.58997)$
 $m_1 = m_2 = m_3 = m_4 = 11.50163$
- P1** $p_1 = (5.23923, -4.18858, 0.74966, -3.05669)$
 $p_2 = (6.99881, -2.93659, 5.03338, 3.87619)$
 $m_1 = m_2 = m_3 = 7.73358$
- P2** $p_1 = (13.42254, 58.79478, -73.11858, -91.95015)$
 $p_2 = (81.65928, -68.52173, 8.75578, -95.05353)$
 $m_1 = 49.97454, m_2 = 86.92490, m_3 = 80.22567$
- P3** $p_1 = (10.51284, 6.89159, -7.40660, -2.85795)$
 $p_2 = (6.45709, 2.46635, 5.84093, 1.22257)$
 $m_1 = m_2 = m_3 = 0.52559$
- P4** $p_1 = (95.77004, 31.32025, -34.08106, -9.38565)$
 $p_2 = (94.54738, -53.84229, 67.11107, 45.56763)$
 $m_1 = 83.02643, m_2 = 76.12873, m_3 = 55.00359$
- P5** $p_1 = (31.54872, -322.40325, 300.53015, -385.58013)$
 $p_2 = (103.90430, 202.00974, -451.27794, -435.12848)$
 $p_3 = (294.76653, 252.88958, 447.09194, 311.71630)$
 $m_1 = m_2 = m_3 = m_4 = 4.68481$
- P6** $p_1 = (50.85428, -55.74613, 11.69987, 94.92591)$
 $p_2 = (0.69914, 67.19262, -5.78627, 91.52776)$
 $p_3 = (52.35768, 76.32258, 43.82222, 13.05874)$
 $m_1 = 54.29650, m_2 = 53.54058, m_3 = 55.96814, m_4 = 51.74438$
- P7** $p_1 = (62.80274, -49.71968, -5.53340, -79.44048)$
 $p_2 = (48.59375, -1.65847, 34.91140, 71.89564)$
 $p_3 = (76.75934, -19.14334, -17.10279, 30.22959)$
 $m_1 = m_2 = m_3 = m_4 = 9.82998$
- P8** $p_1 = (98.04093, 77.37405, 30.53434, -81.88155)$
 $p_2 = (73.67657, -53.78754, 13.69987, 14.20439)$
 $p_3 = (68.14197, -36.48119, 59.89499, -81.79030)$
 $m_1 = 81.44869, m_2 = 94.39003, m_3 = 57.53145, m_4 = 0.40190$
- P9** $p_1 = (76.50219, -72.36197, 10.95225, -99.79612)$
 $p_2 = (99.02723, 27.27133, -25.11907, 86.10825)$

- $p_3 = (64.19420, 13.10011, 18.37737, -29.16095)$
 $m_1 = m_2 = 37.77809, m_3 = m_4 = 36.84323$
- P10** $p_1 = (13.62303, -64.20757, -17.59085, -8.81785)$
 $p_2 = (96.67650, 89.65623, -18.47276, 40.73203)$
 $p_3 = (66.21913, -39.49917, 3.640139, -82.31669)$
 $m_1 = m_3 = 64.67282, m_2 = m_4 = 51.13181$
- P11** $p_1 = (33.74515, 45.72730, 31.15254, -7.47943)$
 $p_2 = (31.36435, -41.50734, 46.47897, 2.04203)$
 $p_3 = (4.59005, 17.07010, 32.65403, 41.93628)$
 $p_4 = (29.51054, -28.25963, 46.17333, -35.08918)$
 $m_1 = m_2 = m_3 = m_4 = m_5 = 5.01213$
- P12** $p_1 = (33.76482, 45.44063, -10.68084, 16.41925)$
 $p_2 = (72.93498, 67.49170, -11.81485, -36.28455)$
 $p_3 = (8.01673, -49.40112, -66.09200, -0.11414)$
 $p_4 = (-86.54188, -97.01228, 68.12494, 32.94875)$
 $m_1 = 98.42704, m_2 = 28.89059, m_3 = 40.51436, m_4 = 75.45643, m_5 = 11.08327$
- P13** $p_1 = (1.58374, 6.86200, -15.06805, -10.63574)$
 $p_2 = (7.54800, -3.36539, 34.57385, 27.52676)$
 $p_3 = (43.36396, -49.27646, -25.35062, -17.68709)$
 $p_4 = (22.58103, 38.31530, -14.67581, -3.08209)$
 $m_1 = m_2 = m_3 = m_4 = m_5 = 2.76340$
- P14** $p_1 = (-89.85270, 69.44839, -96.30496, 14.47549)$
 $p_2 = (-81.61779, 6.89065, 1.76775, 18.39834)$
 $p_3 = (-89.80789, 24.32486, 48.73341, 0.74094)$
 $p_4 = (-43.20198, -85.34635, 92.38148, 93.84802)$
 $m_1 = 22.21430, m_2 = 15.84324, m_3 = 34.80431, m_4 = 27.53390, m_5 = 29.19823$
- P15** $p_1 = (94.79774, -70.04005, -84.77221, 36.09812)$
 $p_2 = (-42.15872, -36.33754, -14.72331, -41.24018)$
 $p_3 = (73.77293, 88.37064, 33.47296, -24.17542)$
 $p_4 = (81.85638, 77.17370, -62.39774, -6.89737)$
 $m_1 = m_2 = m_3 = 1.30619, m_4 = m_5 = 1.26692$

- P16** $p_1 = (69.70234, 62.68042, 25.44429, -97.78603)$
 $p_2 = (-65.98494, -85.19920, 98.05702, -70.89141)$
 $p_3 = (-26.75642, -30.42288, -26.84633, 14.81944)$
 $p_4 = (-69.44800, 56.74842, -32.23649, 96.45829)$
 $m_1 = m_2 = m_3 = m_4 = m_5 = 87.00572$
- P17** $p_1 = (-45.80756, 95.63842, -55.04954, 44.01174)$
 $p_2 = (36.09562, 52.66752, -11.22354, -87.48918)$
 $p_3 = (-4.90798, 41.11273, 14.29379, 2.15944)$
 $p_4 = (49.48233, 40.26756, -23.16581, -96.89362)$
 $m_1 = m_2 = m_3 = m_4 = m_5 = 56.97318$
- P18** $p_1 = (-18.90057, -97.14671, 44.69176, -16.67528)$
 $p_2 = (-70.86315, -81.27489, -3.71628, 18.79403)$
 $p_3 = (-89.53092, 50.02356, 33.39784, -51.66031)$
 $p_4 = (-96.59097, -34.80215, -83.24353, 44.73888)$
 $m_1 = m_2 = m_3 = m_4 = m_5 = 43.87459$
- P19** $p_1 = (-88.70322, 37.98826, 62.19352, -35.86433)$
 $p_2 = (-58.60617, -58.60074, -83.75298, 61.78210)$
 $p_3 = (-83.73607, 46.98912, 67.44602, 78.40612)$
 $p_4 = (-96.41508, 71.69925, -14.47818, -61.82390)$
 $m_1 = m_2 = m_3 = m_4 = m_5 = 16.73899$
- P20** $p_1 = (-3.43584, 4.73492, 17.31242, 61.53467)$
 $p_2 = (12.12233, 32.23256, 87.57836, -58.25073)$
 $p_3 = (-38.67209, -54.27020, 21.15570, 79.15640)$
 $p_4 = (-90.90573, -79.70266, -88.26463, -66.00973)$
 $p_5 = (-34.40043, -88.73043, 84.41781, -4.21221)$
 $m_1 = 54.36459, m_2 = 30.96600, m_3 = 51.03652,$
 $m_4 = 16.03115, m_5 = 2.25657, m_6 = 59.45020$
- P21** $p_1 = (-9.85384, 15.70678, 80.94234, -84.96387)$
 $p_2 = (90.11707, -74.59469, -70.73997, 54.32748)$
 $p_3 = (-55.84212, -34.47531, -87.20597, -27.73882)$
 $p_4 = (16.72808, 64.83574, -31.16733, 63.94189)$
 $p_5 = (-42.62943, 49.91058, -46.12974, 59.76096)$
 $m_1 = 42.61768, m_2 = 22.13590, m_3 = 34.87263,$
 $m_4 = 54.00634, m_5 = 79.54844, m_6 = 87.50131$

P22 $p_1 = (35.27512, 36.08798, -89.66662, 18.22907)$
 $p_2 = (-32.58939, 14.45447, 86.93898, -47.20827)$
 $p_3 = (-76.40210, -62.22587, -63.59955, 41.03465)$
 $p_4 = (-2.30248, 0.45058, -76.74256, -64.19292)$
 $p_5 = (-88.80252, 18.06504, -6.53891, 49.34535)$
 $m_1 = m_2 = m_3 = m_4 = m_5 = m_6 = 82.87370$

P23 $p_1 = (-99.20747, -68.16217, 95.24772, 68.87644)$
 $p_2 = (-95.09224, 78.51258, -82.38270, 20.36899)$
 $p_3 = (-56.04092, 22.93681, -72.82681, 96.81954)$
 $p_4 = (78.53840, -86.40143, -82.49674, -57.42855)$
 $p_5 = (13.70265, 77.87278, 99.79126, 8.31677)$
 $m_1 = 63.23680, m_2 = 86.48449, m_3 = 44.51361,$
 $m_4 = 79.73599, m_5 = 74.43246, m_6 = 70.11421$

P24 $p_1 = (-70.26380, 96.72681, 21.66556, -37.40054)$
 $p_2 = (-13.45985, 2.12040, 3.20198, 91.44246)$
 $p_3 = (-62.59164, -29.93690, -22.16595, -58.38466)$
 $p_4 = (-67.60797, -83.23480, 18.49429, 8.94427)$
 $p_5 = (-34.70936, -62.59326, -60.71318, 2.77450)$
 $m_1 = 94.53242, m_2 = 64.45092, m_3 = 74.74299,$
 $m_4 = 10.63129, m_5 = 31.77881, m_6 = 23.93819$

A.2 Energy and mass scans

Figure 7 $p_1 = (27.95884, 25.55639, -29.88288, -2.17433)$
 $p_2 = (27.45521, -7.81292, 3.19651, 6.05088)$
 $6.05088 \leq m_1 = m_2 = m_3 \leq 31.53414$

Figure 8 $p_1 = (67.40483, 49.44993, -20.67085, 48.63654)$
 $p_2 = (54.64295, -58.23071, 9.55042, -16.59411)$
 $p_3 = (41.37620, 11.75178, -40.77655, -8.25014)$
 $2.33822 \leq m_1 = m_2 = m_3 = m_4 \leq 70.14658$

Figure 9 $p_1 = \sqrt{\lambda}(-15.22437, -26.74156, 6.65483, 29.13661)$, $\lambda \in [1, 30]$,
 $p_2 = (-91.22611, -63.97875, 55.07507, -52.90153)$
 $p_3 = (0.95105, 75.90791, -10.13814, -88.40860)$
 $p_4 = (43.04908, 77.11321, -50.69469, -7.60198)$
 $m_1 = 49.12560, m_2 = 57.87487, m_3 = 26.47098, m_4 = 0.42094, m_5 =$
 62.31320

Figure 10 $p_1 = \sqrt{\lambda}(-51.76504, -81.75539, -46.42422, -40.15540)$, $\lambda \in [1, 30]$,
 $p_2 = (-63.76533, -2.53015, 16.27485, 69.16770)$
 $p_3 = (-78.50262, 46.32052, 13.19246, -54.00166)$
 $p_4 = (25.40582, 81.48058, 39.11105, 93.24648)$
 $m_1 = 78.45208, m_2 = 42.71315, m_3 = 91.94256, m_4 = 61.59730, m_5 = 16.75672$

References

- [1] S. Catani and M. H. Seymour, “The Dipole formalism for the calculation of QCD jet cross-sections at next-to-leading order,” *Phys. Lett. B* **378**, 287 (1996) [hep-ph/9602277].
- [2] D. E. Soper, “QCD calculations by numerical integration,” *Phys. Rev. Lett.* **81** (1998) 2638 [hep-ph/9804454].
- [3] D. E. Soper, “Techniques for QCD calculations by numerical integration,” *Phys. Rev. D* **62** (2000) 014009 [hep-ph/9910292].
- [4] D. E. Soper, “Choosing integration points for QCD calculations by numerical integration,” *Phys. Rev. D* **64** (2001) 034018 [hep-ph/0103262].
- [5] M. Kramer and D. E. Soper, “Next-to-leading order numerical calculations in Coulomb gauge,” *Phys. Rev. D* **66** (2002) 054017 [hep-ph/0204113].
- [6] A. Ferroglia, M. Passera, G. Passarino and S. Uccirati, “All purpose numerical evaluation of one loop multileg Feynman diagrams,” *Nucl. Phys. B* **650** (2003) 162 [hep-ph/0209219].
- [7] Z. Nagy and D. E. Soper, “General subtraction method for numerical calculation of one loop QCD matrix elements,” *JHEP* **0309** (2003) 055 [hep-ph/0308127].
- [8] Z. Nagy and D. E. Soper, “Numerical integration of one-loop Feynman diagrams for N-photon amplitudes,” *Phys. Rev. D* **74** (2006) 093006 [hep-ph/0610028].
- [9] M. Moretti, F. Piccinini and A. D. Polosa, “A Fully Numerical Approach to One-Loop Amplitudes,” arXiv:0802.4171 [hep-ph].
- [10] W. Gong, Z. Nagy and D. E. Soper, “Direct numerical integration of one-loop Feynman diagrams for N-photon amplitudes,” *Phys. Rev. D* **79** (2009) 033005 [arXiv:0812.3686 [hep-ph]].
- [11] W. Kilian and T. Kleinschmidt, “Numerical Evaluation of Feynman Loop Integrals by Reduction to Tree Graphs,” arXiv:0912.3495 [hep-ph].
- [12] S. Becker, C. Reuschle and S. Weinzierl, “Numerical NLO QCD calculations,” *JHEP* **1012** (2010) 013 [arXiv:1010.4187 [hep-ph]].

- [13] S. Becker, C. Reuschle and S. Weinzierl, “Efficiency Improvements for the Numerical Computation of NLO Corrections,” *JHEP* **1207** (2012) 090 [arXiv:1205.2096 [hep-ph]].
- [14] S. Becker and S. Weinzierl, “Direct contour deformation with arbitrary masses in the loop,” *Phys. Rev. D* **86** (2012) 074009 [arXiv:1208.4088 [hep-ph]].
- [15] G. Bevilacqua, M. Czakon, M. V. Garzelli, A. van Hameren, A. Kardos, C. G. Papadopoulos, R. Pittau and M. Worek, “Helac-nlo,” *Comput. Phys. Commun.* **184**, 986 (2013) [arXiv:1110.1499 [hep-ph]].
- [16] F. Cascioli, P. Maierhofer and S. Pozzorini, “Scattering Amplitudes with Open Loops,” *Phys. Rev. Lett.* **108** (2012) 111601 [arXiv:1111.5206 [hep-ph]].
- [17] G. Cullen *et al.*, “GOSAM-2.0: a tool for automated one-loop calculations within the Standard Model and beyond,” *Eur. Phys. J. C* **74**, no. 8, 3001 (2014) [arXiv:1404.7096 [hep-ph]].
- [18] T. Gleisberg, S. Hoeche, F. Krauss, M. Schonherr, S. Schumann, F. Siegert and J. Winter, “Event generation with SHERPA 1.1,” *JHEP* **0902**, 007 (2009) [arXiv:0811.4622 [hep-ph]].
- [19] S. Frixione and B. R. Webber, “The MC and NLO 3.4 Event Generator,” arXiv:0812.0770 [hep-ph].
- [20] J. Alwall *et al.*, “The automated computation of tree-level and next-to-leading order differential cross sections, and their matching to parton shower simulations,” *JHEP* **1407**, 079 (2014) [arXiv:1405.0301 [hep-ph]].
- [21] G. Passarino, “An Approach toward the numerical evaluation of multiloop Feynman diagrams,” *Nucl. Phys. B* **619** (2001) 257 [hep-ph/0108252].
- [22] C. Anastasiou, S. Beerli and A. Daleo, “Evaluating multi-loop Feynman diagrams with infrared and threshold singularities numerically,” *JHEP* **0705** (2007) 071 [hep-ph/0703282].
- [23] S. Becker and S. Weinzierl, “Direct numerical integration for multi-loop integrals,” *Eur. Phys. J. C* **73** (2013) 2321 [arXiv:1211.0509 [hep-ph]].
- [24] S. Catani, T. Gleisberg, F. Krauss, G. Rodrigo and J. C. Winter, “From loops to trees by-passing Feynman’s theorem,” *JHEP* **0809** (2008) 065 [arXiv:0804.3170 [hep-ph]].
- [25] G. Rodrigo, S. Catani, T. Gleisberg, F. Krauss and J. C. Winter, “From multileg loops to trees (by-passing Feynman’s Tree Theorem),” *Nucl. Phys. Proc. Suppl.* **183** (2008) 262 [arXiv:0807.0531 [hep-th]].
- [26] I. Bierenbaum, S. Catani, P. Draggiotis and G. Rodrigo, “A Tree-Loop Duality Relation at Two Loops and Beyond,” *JHEP* **1010** (2010) 073 [arXiv:1007.0194 [hep-ph]].

- [27] I. Bierenbaum, S. Buchta, P. Draggiotis, I. Malamos and G. Rodrigo, “Tree-Loop Duality Relation beyond simple poles,” *JHEP* **1303** (2013) 025 [arXiv:1211.5048 [hep-ph]].
- [28] I. Bierenbaum, P. Draggiotis, S. Buchta, G. Chachamis, I. Malamos and G. Rodrigo, “News on the loop–tree Duality,” *Acta Phys. Polon. B* **44** (2013) 2207.
- [29] S. Buchta, G. Chachamis, P. Draggiotis, I. Malamos and G. Rodrigo, “On the singular behaviour of scattering amplitudes in quantum field theory,” *JHEP* **1411** (2014) 014 [arXiv:1405.7850 [hep-ph]].
- [30] S. Buchta, G. Chachamis, I. Malamos, I. Bierenbaum, P. Draggiotis and G. Rodrigo, “The loop-tree duality at work,” *PoS LL* **2014** (2014) 066 [arXiv:1407.5865 [hep-ph]].
- [31] S. Buchta, PhD thesis, Universitat de València, 2015, “Theoretical foundations and applications of the Loop-Tree Duality in Quantum Field Theories,” [arXiv:1509.07167 [hep-ph]].
- [32] S. Buchta, G. Chachamis, P. Draggiotis, I. Malamos and G. Rodrigo, “Towards a Numerical Implementation of the Loop-Tree Duality Method,” *Nucl. Part. Phys. Proc.* **258-259** (2015) 33 [arXiv:1509.07386 [hep-ph]].
- [33] R. J. Hernández-Pinto, G. F. R. Sborlini and G. Rodrigo, “Gauge theories in four dimensions,” arXiv:1506.04617 [hep-ph].
- [34] T. Hahn and M. Perez-Victoria, *Comput. Phys. Commun.* **118**, 153 (1999) [hep-ph/9807565].
- [35] T. Hahn, “CUBA: A Library for multidimensional numerical integration,” *Comput. Phys. Commun.* **168** (2005) 78 [hep-ph/0404043].
- [36] J. Berntsen, T. O. Espelid, A. Genz, ”An Adaptive Algorithm for the Approximate Calculation of Multiple Integrals” *ACM Trans. Math. Softw.* **17** (1991) 437-451.
- [37] J. Berntsen, T. O. Espelid, A. Genz, ”An Adaptive Multidimensional Integration Routine for a Vector of Integrals” *ACM Trans. Math. Softw.* **17** (1991) 452-456.
- [38] G. P. Lepage, “Vegas: An Adaptive Multidimensional Integration Program,” Report No CLNS-80/447.
- [39] Wolfram Research, Inc., “Mathematica,” Version 10.0, (2015).
- [40] S. Borowka, G. Heinrich, S. P. Jones, M. Kerner, J. Schlenk and T. Zirke, “SecDec-3.0: numerical evaluation of multi-scale integrals beyond one loop,” arXiv:1502.06595 [hep-ph].